Tracking interlinked microbial and geochemical succession over decades in landfilled municipal solid waste

Kimber E. Munford[a]#, Daniel S. Grégoire[b], Laura A. Hug[a]

[a]Department of Biology, University of Waterloo, Waterloo, Ontario, Canada

[b]Department of Chemistry, Carleton University, Ottawa, Ontario, Canada

Running Title: Microbial and geochemical succession in a landfill

#Address correspondence to Kimber E. Munford, kmunford@uwaterloo.ca.

Abstract

Landfills are heterogeneous built environments embedded in natural freshwater systems. They pose increasing risks of groundwater contamination from metal-bearing leachates over time. The interlinked succession of waste decomposition processes, microbial community membership and metal cycling across a landfill's lifespan have not been explored, reducing our ability to predict the long-term environmental impacts of landfills. Working with 1,647 metagenome-assembled genomes from a single landfill, from samples spanning over 39 years of waste decomposition, we identified changes in landfill biogeochemistry and connected these changes to shifts in microbial community composition and predicted functions over time. Comparing between Older (aged 31 – 39 years) and Newer (aged 3 – 20 years) waste cells identified significant shifts in the availability of labile carbon, redox-associated processes, and concentrations of mobile metals – all higher in Newer cells. Newer cells were dominated by chemoorganoheterotrophs, while Older cells contained higher proportions of chemolithoautotrophs and organisms with higher metabolic versatility. Metal resistance and metal cycling genes were significantly more abundant in Older cells. Using geochemistry data from time of filling to present and microbial membership across six landfill cells of different ages, we developed a conceptual model of landfill characteristics across time. This model connects redox conditions and metal fate, highlighting leachate recirculation as a key process impacting many geochemical parameters and defining site chemistry. Our work highlights the substantial changes occurring over the stabilization phase and provides a conceptual framework for understanding this critical, final stage in a landfill's life cycle.

Importance

Aging landfills pose significant risks to environmental stability and are currently poorly modeled beyond ~20 years. Our examination of a single landfill across 39 years of waste degradation was a unique opportunity to examine the impact of time within a connected system. Our work connects geochemical data, microbial membership and predicted function, as well as physical processes (*e.g.*, leachate recirculation). Our conceptual model interlinks these facets across the lifespan of a landfill, providing an empirical data-based model of landfill aging. Previous models were extrapolated from younger waste and did not include the microbial dimension – a critical facet of the landfill ecosystem. Our model clarifies processes taking place in older wastes (30+ years), including oxygen infiltration, that have important implications for methane emission and metal mobility and fate over the longer-term.

Keywords

Landfill, municipal solid waste, landfill leachate, metagenomics, metals, biogeochemistry, leachate recirculation, microbial ecology

1.0 Introduction

Landfills are utilized across the globe to store both residential and non-residential waste, including metals from construction waste, household refuse, and electronic waste. Landfills contribute to environmental and human health concerns over the course of their expected life spans, including long-term methane emissions, punctuated and long-term groundwater contamination, and variable potential for leaching of heavy metals or other pollutants, under fluctuating redox conditions (1, 2).

Landfill refuse is generally buried in a sequential series of cells, which are each filled over a span of several years (2, 3) and expected to stably house the refuse for decades. Once closed, landfill cells go through a predictable set of biogeochemical phases as organic matter (OM) is decomposed by microbes. In phase 1 (aerobic), OM is rapidly metabolized through aerobic processes (3, 4). This phase is brief (1-2 years) as remaining oxygen is depleted via microbial respiration, leading to anoxic conditions. In phase 2 (anaerobic acid), hydrolytic, fermentative, and acetogenic bacteria continue metabolizing OM and produce organic acids, leading to decreases in pH and an overall decrease in OM (5). Phase 2 is followed by a rapid methanogenic phase (phase 3), where methane production peaks, and a slow methanogenic phase (phase 4). Methane production slows in phase 4 as labile OM sources are depleted and methanogenesis shifts to reliance on the downstream products from other organisms' hydrolysis of polymeric carbon sources (1, 3, 6). The duration of phases 2-4 are highly variable, and dependent on substrate conditions and climate, which impact the speed of OM breakdown (4, 6). Phase 4 can last for decades. It has been proposed that, beyond phase 4, landfills will enter a stabilization phase (phase 5). Some have defined this phase by the transition to microbial activity on more recalcitrant carbon sources (*e.g.*, humic and fulvic acids) (4, 6–8). At this point, due to

reduced microbial demand, oxygen entering landfill cells via passive diffusion can lead to increased oxygen availability and more oxidizing conditions.

Shifts in redox conditions over the landfill life cycle are expected to impact microbe-metal interactions and metal mobility as landfills age (3, 4, 9). Despite this, few have investigated the differences in biogeochemical conditions between older and newer landfill cells, particularly with respect to metal resistance and metal cycling (10, 11). Overwhelmingly, existing studies compare different landfills rather than cells within one landfill, which may impact comparisons of underlying chemistry. Additionally, they typically focus on carbon cycling and greenhouse gas production, omitting metals. Studies have found that the early stages of the landfill life cycle are characterized by rapid (over 5-10 years) decreases in labile organic substrates (5, 6, 12). Others have shown that landfills experience a shift from microbial communities associated with the breakdown of OM to those dominated by lithoautotrophs over time (10, 13). What is less understood is how this microbial community succession impacts metal cycling and leaching. Some studies report higher metal concentrations in newer landfills, while others predict that metals may be mobilized in the later phases of the landfill life cycle (3, 10, 11). Increasingly oxidizing conditions in phase 5 can lead to oxidation of reduced sulfides, releasing metals and reducing pH (3, 14). Additionally, organic substrates (*e.g.,* humic or fulvic substances) remaining in waste during the stabilization phase (phase 5) can form soluble complexes or colloids with metals, increasing metal mobility (3, 4).

Here we investigate microbial community structure and associated functional genes between Older (aged 31 – 39 years) and Newer (aged 3 – 20 years) landfill cells from a landfill in the Northeastern U.S. We connect these examinations of metabolic guilds and microbe-metal interactions with changes in leachate chemistry collected over more than three decades. A

previous study by Grégoire *et al.* (2023) looked at microbiological and geochemical evidence for methane cycling in the same system, where their highlighted oxygen infiltration into older landfill cells. As a result, our study focused on differences in microbial communities and leachate geochemistry over time, focusing on major microbial metabolic processes involved in and controlled by redox cycling. We hypothesized that older landfill cells would host microbial communities whose functional genes had a higher potential for utilization of inorganic electron acceptors and cycling of metals while newer landfill cells would have microbial communities with functional genes more strongly associated with anaerobic fermentative processes.

2.0 Results

2.1 Site description and sampling

The sampled site is a municipal landfill located in the northeastern United States (NEUS), site anonymity requested by site engineers. The site is composed of six landfill cells (A, B, C, D, E, and F), two of which are divided into sub-cells (D into D1 and D2, and F into F1 and F2), each equipped with leachate collection systems. Landfill cells were broadly separated by age into "Older" (cells A, B, and C; aged 31 – 39 years), "Intermediate" (cells D1 and D2; aged 24 – 26 years), and "Newer" (cells E, F1, and F2, 3 – 20 years) based on their predicted landfill phase (Older = phase 4-5, Newer = phase 2-3). Landfill phases were determined by Grégoire *et al.* 2023 (1) in their work investigating methane cycling at the site, utilizing measured biological oxygen demand (BOD) and chemical oxygen demand (COD) to assign phases. Leachate samples were collected in 2019 for sequencing and metagenomic analysis (see Methods, (1)). The site owners enthusiastically provided historic and current leachate geochemistry records under a Freedom Of Information Act (FOIA) request. Notably, microbial samples come from a single point in time (sampling in 2019) whereas leachate chemistry data spans the lifetime of the cells. As a result, microbial analyses focus on comparisons between the oldest ("Older") and youngest ("Newer") cells. Integrations of microbial and leachate chemistry data draw on the entire dataset.

2.2 Taxonomic composition of microbial communities

Starting from 1,647 total bins, dereplication was performed at 99% similarity to compare shared populations across cells, yielding 1,178 metagenome-assembled genomes (MAGs) across all eight metagenomes (all cells and sub-cells). Fewer total MAGs (>70% completion, <10% contamination) were detected in Older landfill cells (138 ± 48) than Intermediate (245 ± 34.7) or Newer cells (248 ± 42.7), with 93 MAGs in cell A, 188 in cell B, 134 in cell C, 220 in D1, 269 in D2, 210 in E, 294 in F1, and 239 in F2. Only 32 dereplicated MAGs were shared among all three

130 age groups, and only 5 dereplicated MAGs were shared between Older and Newer cells to the
131 exclusion of Intermediate cells (Figure 1c). Beyond limited shared MAGs, there were large
132 taxonomic differences between communities from Older and Newer cells, based on taxonomic
133 assignment by GTDB-tk (release 226) (15) and from a phylogenomic tree encompassing MAGs
134 from all samples (Figure 1a). Taxonomic assignment, trees, and all subsequent analyses were
135 performed using the set of 1,647 non-dereplicated MAGs to capture cell-by-cell differences (see
136 Methods). Of the 1,647 MAGs in the dataset, only 77 had too few hits to the required marker
137 genes to be included in the tree. Removed MAGs, on average, had a relative abundance of
138 <0.5%. Most of these 77 MAGs (63.6%) were within the Halobacteriota (22 MAGs) or placed
139 within groups with small genomes that may be missing key markers (Patescibacteriota [18
140 MAGs], Nanobdellota [7 MAGs], Micrarchaeota [2 MAGs]). A full table of taxonomic
141 classifications, relative abundance, tree membership, completeness and contamination, and
142 dereplication cluster membership is available on the Open Science Framework (OSF)
143 (https://doi.org/10.17605/OSF.IO/MSDB8)(16).

144 Overall, Older cells had lower Shannon Diversity (3.70 ± 0.640) than Intermediate (4.94
145 ± 0.0322) or Newer (4.63 ± 0.0445) cells. Older cells had a strong enrichment in members of the
146 families Gallionellaceae and Sulfurimonadaceae, with enrichment in Arcobacteraceae in cell C.
147 Collectively, members of the Gallionellaceae, Sulfurimonadaceae, and Arcobacteraceae
148 represented 50.3% relative abundance in cell A, 30.0% in cell B, and 57.8% in cell C (Figure
149 1b), highlighting the overall lower microbial diversity in Older cells. The Gallionellaceae family
150 consisted of 15 dereplicated MAGs across one unidentified (JAQTOM01 [1 MAG]) and two
151 identified genera (*Gallionella* [10 MAGs] and *Sideroxyarcus* [4 MAGs]), and comprised 24.4%
152 (3 MAGs), 26.7% (7 MAGs), and 11.5% (6 MAGs) in cells A, B, and C, respectively. Members

153 of the Gallionellaceae were also present in D1 (0.327% [2 MAGs]) and F1 (0.371% [1 MAG]),
154 but at lower abundance than in Older cells. The family Sulfurimonadaceae was represented by 24
155 dereplicated MAGs across 2 genera (*Sulfuricurvum* [12 MAGs] and *Sulfurimonas* [12 MAGs]) in
156 all cells (Figure 1b, Table S1), and comprised 25.9% (6 MAGs), 3.36% (6 MAGs), and 1.91% (7
157 MAGs) in cells A, B, and C, respectively. Relative abundance of members of the
158 Sulfurimonadaceae was <1% in all Intermediate and Newer cells (1 MAG in D1, 1 in D2, 8 in E,
159 and 1 in F1). Arcobacteraceae was the most abundant family in any one sample, comprising
160 44.4% of the microbial community in cell C. Within cell C, three dereplicated Arcobacteraceae
161 MAGs were present, two from the genus *Aliarcobacter* (44.0%) and one unidentified
162 (CAIJNA01 [0.495%]). Arcobacteraceae were not detected in cells A or B but were present at
163 lower abundances in cells D2 (6.22% [4 MAGs]), E (5.19% [1 MAG]), and F1 (0.548% [1
164 MAG]).

165 Contrastingly, Newer cells showed enrichments in members of the families
166 Dysgonomonadaceae and Cloacimonadaceae. Dysgonomonadaceae consisted of 17 dereplicated
167 MAGs across 2 identified genera (*Proteiniphilum* [10 MAGs] and *Petrimonas* [2 MAGs]) and 5
168 MAGs unidentified at the genus level. Relative abundance of MAGs in the genus *Proteiniphilum*
169 was 3.04% (5 MAGs), 7.45% (7 MAGs), and 17.2% (10 MAGs) in E, F1, and F2, respectively,
170 while it was below 1% in Older cells (3 MAGs in C only) and D1 (1 MAG), but slightly more
171 abundant in D2 (2.32% [3 MAGs]). Relative abundance of MAGs in the genus *Petrimonas* was
172 2.12% (5 MAGs), 0.392% (7 MAGs), and 2.00% (10 MAGs) in E, F1, and F2, respectively, and
173 less than 1% in Older (1 MAG in A and 3 in C) and Intermediate (1 MAG in D1 and 3 in D2)
174 cells. In total, relative abundance of all unidentified members of the Dysgonomonadaceae family
175 were 3.66% (3 MAGs), 0.319% (2 MAGs), and 1.61% (4 MAGs) in E, F1, and F2, respectively,

176 and they were only detected in one other cell (D2 at 0.393% [2 MAGs]). The family
177 Cloacimonadaceae consisted of 18 dereplicated MAGs, most of which were unidentified at the
178 genus level (UBA5456 [10 MAGs]), with the identified genera being *Syntrophosphaera* (4
179 MAGs) and *Cloacimonas* (4 MAGs). Relative abundance of members of the Cloacimonadaceae
180 was 5.38% (10 MAGs), 12.8% (9 MAGs), and 12.7% (6 MAGs) in E, F1, and F2, respectively.
181 Cloacimonadaceae abundances were lower in Intermediate cells, with 2.21% in D1 (3 MAGs)
182 and 2.80% in D2 (6 MAGs), and at less than 1% in all Older cells (1 MAG in A and 2 in C).

183 As shown above, Intermediate samples tended to be variable, with microbial composition
184 in D1 more strongly resembling Older cells, while composition in D2 was closer to Newer cells.
185 Interestingly, both subcells of cell D were enriched in families whose members are typically very
186 small cells (≤0.8 μm) with reduced genomes (17, 18). This included the family
187 Profunditerraquicolaceae (D1: 10.9%, D2: 0.749%) with 43 MAGs from 2 identified genera
188 (*Undivivens* [D1: 0.449%, D2: 0.242%] and *Sherwoodlollariibacterium* [D1:0.353%, D2:
189 0.241%]), each represented by 1 dereplicated MAG, and 41 MAGs from unidentified genera
190 (D1: 10.14% [24 MAGs], D2: 0.266% [2 MAGs]). Members of the Profunditerraquicolaceae
191 were also found in Older (30 MAGs in A, B, and C) and Newer (2 MAGs in F1 only) cells at less
192 than 1% relative abundance in all cells except B, where relative abundance was 9.47% (22
193 MAGs).

194 Similarly, two families within the Patescibacteriota phylum were also enriched in the
195 Intermediate (D) cells. Members of the Minisyncoccaceae, represented by 17 MAGs across 2
196 identified genera (*Microsyncoccus* [3 MAGs] and *Minisyncoccus* [2 MAGs]) and 4 unidentified
197 genera (12 MAGs), had 2.94% (5 MAGs) and 10.6% (8 MAGs) relative abundance in D1 and
198 D2, respectively. Members of Minisyncoccaceae were also present in Newer cells, with 0.762%

199 (1 MAG), 3.44% (6 MAGs), and 2.97% (5 MAGs) relative abundance in E, F1, and F2,
200 respectively. Relative abundance of Minisyncoccaceae was less than 2% in all Older cells,
201 detected only in B and C with 3 MAGs in each cell. Finally, an uncultured order (UBA6257) in
202 the Patescibacteriota phylum (18 MAGs) had high relative abundance in cell D, with 7 MAGs in
203 D1 and 3 MAGs in D2, accounting for 9.61% and 1.04% relative abundance, respectively.
204 MAGs from UBA6257 were also present in Older (B: 8.75% [4 MAGs], C: 0.248% [1 MAG])
205 and Newer (E: 5.45% [7 MAGs], F1: 0.723% [1 MAG], F2: 0.178% [2 MAGs]) cells.

206 Although there were some similarities at the Family level, few dereplicated MAGs (5
207 total) were shared between Older and Newer cells (Figure 1c). In contrast, 42% of dereplicated
208 MAGs in Intermediate cells were shared with Newer, Older, or both. Thus, Intermediate cells
209 reflect a transitionary state between Older and Newer, highlighting how few taxa can persist
210 following transition between landfill phases. Due to the clear distinction between microbial
211 community compositions in Older and Newer cells, we opted to focus on comparisons between
212 these two age groups for our downstream analyses.

213 **2.3 Microbial diversity and functional genes**

214 There were substantial differences in predicted functional capacity for microbial
215 communities in landfill cells of different ages. In total, we examined 200 different functional
216 gene groups and pathways. We utilized Distilled and Refined Annotation of Metabolism
217 (DRAM) v1.0 (19) to annotate MAGs, focusing on ninety-three functional gene groups and
218 pathways, covering central metabolism, carbohydrate-active enzymes (CAZymes), conversion of
219 short-chain fatty acids (SCFAs) and alcohols, methanogenesis and methanotrophy, nitrogen
220 cycling, and sulfur cycling. Annotations from four functional groups were identified using
221 FeGenie (20), focusing on iron cycling. Ten more were annotated with an As metabolism and

222 resistance pipeline from Dunivin *et al.* (21), and 93 were derived from BacMetScan (22),
223 covering microbial metal interactions (respiration and resistance). Genes which contributed to
224 functional gene categories across the different annotation tools are listed in Table S2. Only genes
225 which were significantly different at $p < 0.05$ are reported here.

226 To investigate differences in functional potential between cells of differing ages, we
227 integrated all annotations into a presence-absence table for all functional genes, groups, or
228 pathways (available on the Open Science Framework at
229 https://doi.org/10.17605/OSF.IO/MSDB8) (16). DRAM estimates coverage of metabolic
230 pathways and completion of electron transport chain (ETC) complexes based on the percentage
231 of genes recovered. For our presence-absence assessment, we considered pathways and ETC
232 complexes to be present when DRAM's estimate was >70% for a given MAG. Then, abundance
233 of functional genes was calculated by summing the relative coverage of all MAGs that possessed
234 a given functional gene, group, or pathway within a cell, representing the proportion of the
235 microbial community with the encoded potential for a given function.

236 Across the full dataset of 1,647 MAGs, only 6 MAGs (from 0.107 to 0.730% relative
237 abundance) had no functional gene hits with the 70% completion cutoff, including for central
238 metabolic pathways. Four of these MAGs were members of the Patescibacteriota phylum, and
239 two were members of the archaeal phylum Nanobdellota (formerly "Nanoarchaeota"). Members
240 of both of these groups live as symbionts on prokaryotic hosts, lacking portions of some
241 pathways essential for independent life (18, 23, 24). Genomes for these organisms ranged from
242 70.8 – 78.5% completion, so it is also possible that core metabolic genes were absent from our
243 annotations due to incomplete genomes.

We investigated differences in functional gene and pathway abundance and prevalence between Older and Newer cells using Wilcoxon rank sum tests ($p < 0.05$) (Table S2). To explore the fermentative capacity of the microbial communities, we investigated the presence or absence of Complexes I - V of the electron transport chain and DRAM annotations associated with the breakdown of SCFAs and carbohydrates (CAZymes).

Complex IV of the ETC is associated with transfer of electrons to oxygen, the final electron acceptor in aerobic respiration, so a lack of this complex indicates likely anaerobic respiration. The absence of Complexes I - IV of the ETC indicates that an organism is likely an obligate fermenter. Overall, we found that 7 out of 8 Complexes I - IV of the electron transport chain were significantly more abundant in Older cells, including both low and high affinity oxidases, indicating that variable oxygen availability in the system supports aerobic metabolisms (Table S2, Figure S1). The relative lack of Complexes I - IV in Newer cells points to fermentative metabolisms and anaerobic respiration as dominant in Newer cells. ATPases also point to differences in metabolic processes between cell ages. F-type ATPases, which were significantly more abundant in Older cells, often couple to an ETC for oxidative phosphorylation, pointing to aerobic respiration when Complexes I - IV are also present. In Newer cells, V/A-type ATPases were significantly more abundant, possibly reflecting maintenance of proton gradients in microbes with low respiratory activity.

Functional gene groups associated with central carbon metabolism and organic matter decomposition also indicated that fermentation was the key metabolic process in Newer cells compared to aerobic processes in Older cells (Figure 2). Older cells had significantly higher abundance of genes or gene groups associated with the reductive pentose phosphate (Calvin) cycle (Older: 59.5 ± 17.7%; Newer: 19.3 ± 8.47%), reductive citrate (Arnon-Buchanon) cycle

267 (Older: 43.1 ± 10.9%; Newer: 22.5 ± 7.99%), glyoxylate cycle (Older: 14.2 ± 19.4%; Newer:
268 2.12 ± 3.46%), and citrate (Krebs) cycle (Older: 60.3 ± 22.4%; Newer: 15.4 ± 14.7%),
269 suggesting importance of both aerobic and anaerobic respiration, as well as carbon fixation in
270 Older cells (Figure 2). Notably, across all samples, genes for the reductive acetyl-CoA (Wood-
271 Ljungdahl) pathway, associated with anaerobic carbon fixation, were very uncommon, at 1.09 ±
272 1.36% in Older cells and 2.75 ± 1.02% in Newer cells.

273 Contrastingly, Newer cells had significantly higher abundance of gene groups associated
274 with breakdown of carbohydrates. These included CAZymes for breaking down complex
275 carbohydrates like pectin, starch, mannans, and xyloglucan, with 10/16 identified CAZymes at
276 significantly higher proportions in Newer cells. The only exceptions were CAZymes for
277 polyphenolics and mixed-linkage glucans, which were at significantly higher abundance in Older
278 cells. The relatively higher abundance of CAZy genes for polyphenolic and mixed-linkage
279 glucans in Older cells may point to more complex carbon sources remaining in Older cells.
280 Additionally, Newer cells had higher abundance of some genes and gene groups associated with
281 the breakdown of SCFAs and alcohols (5 out of 11 genes were significantly different), such as
282 acetate, butyrate, and pyruvate (Figure 2). Enrichment in CAZy genes and genes associated with
283 SCFA breakdown further point to fermentative activity in Newer cells.

284 Finally, there were also significant differences in genes and gene groups associated with
285 methanogenesis and methanotrophy between Older and Newer cells (Table S2; Figure S2).
286 Briefly, genes associated with methane oxidation were significantly more abundant in Older
287 cells, further indicating possible oxygen infiltration alongside remaining methane in Older cells,
288 though overall relative coverage of MAGs with those genes was low (<2%) (Figure S2). Trends

in methanogenesis and methanotrophy were explored in further detail in Grégoire *et al.*, 2023 (1).

Older cells had higher abundance of MAGs predicted to utilize a variety of alternative electron donors and acceptors. Based on DRAM annotations (for nitrogen [N] and sulfur [S]) and FeGenie results (for iron [Fe]), we found that functional genes and gene groups for reduction and oxidation of all three elements were significantly more abundant in Older cells, pointing to metabolic flexibility in Older cells (Figure 3). Notably, genes associated with all steps of denitrification (nitrate -> nitrite [*napA* or *narG* gene] -> nitric oxide [respiratory nitrite reductase gene] -> nitrous oxide [nitric oxide reductase gene] -> nitrogen [nitrous-oxide reductase gene]) were significantly more abundant in Older cells, with abundance of these genes ranging from 11.5-55.9% in Older cells and from 2.63-15.5% in Newer cells (Figure 3). Similarly, abundance of the functional gene groups associated with oxidation of nitrite to nitrate (*nxrA* and *nxrB* genes) (Older: 25.2 ± 26.9%; Newer: 15.5 ± 5.1%) and bacterial/archaeal ammonia oxidation (*amoA* gene) (Older: 1.96 ± 1.71%; Newer: 0.340 ± 0.588%) were also significantly higher in Older cells. One exception was dissimilatory nitrate reduction to ammonia (*nrfA* gene), which was significantly more abundant in Newer cells (Older: 1.96 ± 1.76%; Newer: 19.3 ± 7.47%). Finally, abundance of the nitrogen fixation gene *nifH* was significantly higher in Older cells (Older: 38.7 ± 21.4%; Newer: 7.61 ± 4.13%). Taken together, the primary processes for generating biologically available nitrogen differ between cell age categories. There was evidence for both aerobic and anaerobic processes, including N fixation, in Older cells, whereas genes for dissimilatory nitrate reduction to ammonia, a process common in strongly reducing environments, were more abundant in Newer cells. These results highlight the differing mechanisms of N acquisition for landfill microbiota as landfills age.

312 Functional gene groups for reduction and oxidation of S and Fe followed similar trends.
313 Two functional gene groups for the oxidation or reduction of sulfate were significantly different
314 in abundance between Older and Newer cells. The functional gene group for partial or complete
315 oxidation of thiosulfate to sulfate (including *soxA, soxB, soxX, soxY* and *soxZ*) was highly
316 abundant in Older (22.7 ± 25.5%) cells, in contrast to Newer (4.70 ± 8.14%) cells. Interestingly,
317 the functional gene group for dissimilatory reduction or oxidation of sulfate (*dsrA* or *dsrB*) was
318 also much higher in Older (16.5 ± 9.33%) than Newer (1.84 ± 1.35%) cells (Figure 3).
319 Functional gene groups identified by FeGenie as associated with iron oxidation (Older: 38.5 ±
320 15.5%; Newer: 0.875 ± 1.00%) and possible iron oxidation or reduction (Older: 7.09 ± 2.92%;
321 Newer: 0.890 ± 0.154%) were also significantly more abundant in Older cells (Figure 3; Table
322 S2). The increase in sulfate and iron reduction genes in Older cells relative to nitrate reduction
323 genes in Newer cells may reflect shifts in terminal electron acceptors as substrates are depleted
324 over time. Finally, abundance of arsenic metabolism genes (*e.g.*, *arrA*, *aioA*) were not
325 significantly different between Older and Newer cells across either the Dunivin *et al*. HMM set
326 (21) or via the BacMet database. The heightened abundance of genes or gene groups for both
327 oxidation and reduction of Fe, S, and N compounds in Older cells highlights a greater reliance on
328 alternative electron donors and acceptors in Older cells.

329 Although there were no significant differences in abundance of respiratory arsenic
330 metabolism genes, genes associated with As detoxification and tolerance were significantly
331 different. Abundance of the arsenic methyltransferase *arsM* (Older: 17.3 ± 4.30%; Newer: 4.30 ±
332 1.23%), and two cytoplasmic arsenate reductase genes (thioredoxin-dependent and glutaredoxin-
333 dependent) were also significantly higher abundance in Older cells. Thioredoxin-dependent
334 arsenate reductase was more abundant in general (Older: 17.8 ± 15.3%; Newer: 7.80 ± 5.46%)

335 than glutaredoxin-dependent arsenate reductase (Older: 8.06% ± 5.27%; Newer: 2.41 ± 3.88%).
336 Both are associated with cytoplasmic reduction of As(V) to As(III) so it can be pumped out of
337 the cell via an arsenite efflux pump (*acr3* or *arsB*). Both arsenite efflux pump genes were
338 significantly more abundant in Older cells, with arsenical resistance-3 protein (*acr3*) (Older: 23.6
339 ± 8.96%; Newer: 9.78 ± 2.95%) being more abundant than *arsB*, which was detected through
340 both the Dunivin *et al*. HMM set and BacMetScan. The two annotation tools use different
341 methods to annotate genes (21, 22), and there was little overlap in annotation of *arsB* between
342 the two methods, with 70 MAGs identified as containing *arsB* from the Dunivin *et al*. set and 99
343 from BacMet, but only 4 overlapping between the two. Across both annotation tools, abundance
344 of the gene encoding the arsenite efflux pump (*arsB*) ranged from 1.31 to 8.43% in Older cells
345 and from 0.266 to 5.99% in Newer cells. The arsenic metallochaperone (*arsD*), also significantly
346 more abundant in Older cells (Older: 5.76 ± 1.39%; Newer: 1.84 ± 1.55%), chaperones
347 intracellular As(III) to *arsB*-encoded efflux pumps. Higher relative abundance of genes that
348 encode various parts of the As detoxification system point to more prevalent As-resistance in
349 Older cells relative to Newer cells. Additionally, the phosphate-transporting ATPase (*pstB*),
350 which can bring As(V) into cells, was also significantly more abundant in Older cells (Older:
351 26.1 ± 9.30%; Newer: 4.36 ± 6.21%), indicating the possibility for increased uptake of As in
352 Older cells as a consequence of P scavenging.

353 We also looked for other metal-resistance genes using BacMetScan and the BacMet
354 database, finding that Older cells displayed significantly higher abundance of genes associated
355 with mitigating chromate toxicity (*chrA*, *chrF*), copper resistance and metabolism (*copR*),
356 cobalt-zinc-cadmium resistance (*czcA*), cobalt, cadmium, and nickel transport (*dmeF*), tellurium
357 resistance (*terD*), and repairing DNA damage following chromate, tellurite, or selenite exposure

358 (*ruvB*) (Figure 3; Figure S3). The DNA repair gene encoding ATP-dependent DNA helicase
359 (*ruvB*) was the most abundant of these metal resistance genes (Older: 21.1 ± 12.8%; Newer:
360 0.660 ± 0.843%). All the other metal resistance genes listed above were below 3% relative
361 coverage, and, interestingly, five of six of these (*chrA*, *chrF*, *czcA*, *dmeF*, and *terD*) were not
362 found in any MAGs from Newer cells. The gene encoding the copper resistance regulator (*copR*)
363 was also below 3% abundance on average but present in both Older (2.66 ± 3.10%) and Newer
364 (0.404 ± 0.495%) cells.

365

366 **2.4 Leachate chemistry**

367 Leachate chemical parameters were investigated for the 5 years prior to sampling and the
368 period of filling for individual cells. Key parameters were selected that associate with microbial
369 functions of interest (Table 1, from full set in Table S3). Tables of all leachate chemistry
370 parameters over time have been uploaded to the Open Science Framework
371 (https://doi.org/10.17605/OSF.IO/MSDB8) (16). Further supporting the differential abundance of
372 redox-cycling genes discussed above, conditions were broadly less reducing in Older cells
373 relative to Newer cells (Table 1). BOD and COD were both significantly lower in Older cells in
374 the 5 years prior to sampling, and there was a massive decline in both BOD (from 9629 ± 9940
375 to 71.6 ± 194.2 mg/L) and COD (from 14285 ± 13298 to 446 ± 387 mg/L) since the time of
376 filling, indicating a clear decrease in labile carbon sources (Table 1; Table S3). Total organic
377 carbon (TOC) in leachate was also significantly lower in Older cells in this time window. Other
378 carbon sources were also at significantly lower concentrations in Older cells, including total
379 phenolics, and acetic acid and propionic acid, both SCFAs. The other investigated SCFAs were
380 not statistically significantly different but had overall lower concentrations in Older cells (Table
381 S3). Shifts in BOD, COD, and labile carbon sources over time and between Older and Newer

cells reflect differences in abundance of functional genes related to fermentation and carbon metabolism over time. Interestingly, leachate concentrations of metals (As, Cr, Fe, Ni) and redox-associated parameters (reduced sulfide and ammonia) were significantly higher in Newer cells than Older cells in the 5 years prior to sampling, despite lower abundance of functional genes associated with sulfate reduction and metal resistance in Newer cells (Table S3). This may be linked to sulfate reduction decreasing soluble concentrations of metals in Older cells, with sulfides incorporated into solid waste.

The 5-year window was selected to represent the geochemical conditions that had most recently shaped the microbial communities examined. It remains possible that earlier conditions have exerted a long-term impact on community membership and functional capacity. Leachate concentrations of most metals (Cd, Cr, Co, Cu, Fe, Mn, Ni, Zn) were significantly higher ($p < 0.05$) in Older cells at the time of filling relative to the time of sampling (Table S3). For example, concentrations of Cr in leachate decreased from 160 ± 410 to 6.17 ± 4.12 μg/L from filling to the 5 years prior to sampling, over 25 times lower. Similarly, Fe also decreased to over 25x less, from 849 ± 2960 to 29.4 ± 101 mg/L (Table S3). Microbial communities in Older cells also had significantly higher abundance of functional genes and gene groups associated with resistance to some of these metals (Cr, Cd, Cu, Co, and Zn) and Fe oxidation and reduction, possibly pointing to a link between historic metal concentrations and present-day capacity for microbe-metal interactions.

To develop a picture of changes in overall landfill chemistry over decades, we aggregated leachate chemistry data into 5-year rolling averages. We computed z-scores for each parameter to assess differences in trends over time and clustered parameters into 8 k-means clusters based on an elbow plot of within-cluster sum of squares (Figure S4, Table 2) to combine leachate

chemistry variables into clusters with similar variance over time. We separated these into those associated with key explanatory parameters (conductivity, redox, pH, OM breakdown) and remaining chemical groupings, highlighting changes over time by plotting averaged z-scores (Figure 4, Figures S5-S9). This allowed us to identify key chemical parameters driving changes in landfill conditions. A table of all z-score adjusted and averaged cluster data is available on the Open Science Framework (https://doi.org/10.17605/OSF.IO/MSDB8) (16).

Interestingly, we found that a group of parameters (SO_4^{2-}, Cu, Mg, Ni, Zn) clustered with the historic practice of leachate recirculation at the site, co-varying over time, with all parameters peaking in concentration at around 10 years since cells began filling (Cluster 1, Figure 4). Leachate recirculation occurred off and on within the landfill from 1985 to the end of 2009. To investigate the impact of leachate recirculation as a driver of leachate chemistry, we performed simple linear regressions on z-score-scaled 5-year rolling averages for all cell ages where there was leachate recirculation (Table S4). Parameters significantly influenced ($p < 0.05$) by the amount of recirculated leachate included carbon-associated parameters (BOD_5, COD), some metals (Cu, Cr, Fe, Ni, Zn), Mg, oxidation-reduction potential, and two redox-associated nutrients (nitrite-N, sulfate). Given that leachate recirculation is generally performed to maintain reducing conditions and speed up waste decomposition, increases in BOD_5/COD and decreases in oxidation-reduction potential are to be expected. The increases in metal concentrations may be linked to faster breakdown of waste, mobilizing more metals into solution, in addition to metals being recirculated back into the system.

The largest cluster contained parameters associated with the breakdown of carbon sources (BOD-5, COD, TOC, SCFAs, total phenolics) and some metals (Ca, Cd, Cr, Fe) (Cluster 2, Figure S5). Calcium concentrations and carbon parameters all followed a similar trend, broadly

peaking just prior to the 10-year mark then declining (Figure S5). For Cd, Cr, and Fe, the rise and fall were more gradual, but still present. The peak for this cluster was earlier than the peak for the recirculation-associated group (including Cu, Mg, Ni, and Zn) (Table 2; Figure 4, Figure S5). Contrastingly, oxidation-reduction potential (sole parameter in Cluster 3) displayed a broad dip at 10 years and a slow rise afterward, reflecting potential oxygen infiltration into the aging landfill (Figure S6).

Conductivity was clustered with sulfide, ammonia-N, bicarbonate, As, K, and Na (Table 2). Conductivity and concentrations of ammonia-N, bicarbonate, K, and Na all followed a similar trend with a broad peak between 10 and 20 years (Figure S7). Sulfide and As were less similar, with a bump in concentration just before the 20-year mark (Figure S7). pH only clustered with Mn, both of which peaked at the beginning of the landfill life cycle before dropping off (Figure S8).

The remaining clusters, all depicted in Figure S9, were cobalt alone, nitrite-N alone, and a cluster containing nitrate-N and selenium. Trends in these were more sporadic over time, and total concentrations tended to be low (below 5 mg/L for nitrate-N and nitrite-N and below 1 mg/L for Co and Se).

Results for redox-associated parameters can be explained in the context of redox metabolism broadly. Manganese peaked early in the landfill life cycle, followed by Fe, both of which would likely be released into landfill leachate upon reduction from oxide forms. Then, following the large peak in Fe, there was a small increase in sulfide. This redox cascade is expected, though measured sulfide concentrations were quite low (<15 mg/L).

3.0 Discussion

This study investigated differences in geochemistry and microbial community structure, composition and functional genes in leachate from cells in a municipal solid waste landfill across 39 years of waste deposition. Few studies have explored the chemical and biological conditions in landfill cells in the later phases of decomposition under field conditions (phases 4 and 5) (3, 13). We compared "Older" (aged 31 – 39, phase 4/5) cells and "Newer" (aged 3 – 20, phase 2/3) cells, finding significant differences in microbial community structure and composition as well as microbial functional genes, and connected these differences to the underlying leachate chemistry. To anchor this discussion, we developed a conceptual model synthesizing results from microbial community functional predictions and landfill chemistry modeled over time (Figure 5).

3.1 Microbial contributions across the 5-phase model of the landfill life cycle

This study fills important gaps in our understanding of the role microbial assemblages play in driving leachate chemical changes over the landfill life cycle, particularly in the later phases. In the early phases of the landfill life cycle, one of the key changes is an accumulation of labile organic matter (*e.g.*, organic acids) as microbes break down complex organic material (3, 12). We observed a gradual increase in leachate organic acids (acetic, propionic, butyric, isobutyric, isovaleric, and valeric acid), biological oxygen demand, and chemical oxygen demand from 0-7 years for landfill filling, before a decrease of these parameters to near zero by year 12 (Figure 5b – cluster 2). Similar trends in organic acids and BOD/COD have been found by other authors, who have observed major decreases within 10 years (12) or as little as 4 years (5). Within this first seven years, pH declined substantially due to this accumulation of organic acids, produced from hydrolysis and fermentation of OM during the anaerobic acid phase (phase 2) of the landfill life cycle (3–5). It is expected that organic acids produced in phase 2 then feed

473 the rapid methanogenesis that characterizes phase 3, explaining the overall decline in organic
474 acids and biological and chemical oxygen demand (4).

475 Our microbial samples, collected in 2019, captured two cells transitioning from phase 2
476 to 3 (F1 and F2) and one in phase 3 (E), making up our group of "Newer" cells. These cells had
477 higher Shannon Diversity and higher numbers of MAGs compared to Older cells. Very few
478 MAGs were shared between Older and Newer cells, reflecting differences in geochemical
479 context and shifts in microbial metabolism and survival strategies as landfill waste decomposes
480 over time (3). Due to the overall higher diversity of the microbial communities in Newer cells,
481 only the families Dysgonomonadaceae and Cloacimonadaceae were more relatively abundant
482 than other families across Newer cells (Figure 1b). MAGs from both families encoded a variety
483 of genes associated with carbohydrate-active enzyme (CAZyme) families and with breakdown of
484 SCFA and alcohol conversions. Members of the Dysgonomonadaceae have been found in a
485 variety of environments, including landfills (25–27) and anaerobic digesters (28, 29), and are
486 associated with the breakdown of a variety of organic compounds that are commonly present
487 early in a landfill life cycle. In our data, the genomes of members of the Dysgonomonadaceae's
488 encoded genes for most of the investigated CAZymes as well as for conversions of butyrate,
489 acetate, and pyruvate. Similarly, members of the Cloacimonadaceae have been found in landfills
490 (30) and anaerobic digesters (31, 32), and are associated with syntrophic propionate oxidation
491 (32). Genomes from the Cloacimonadaceae contained fewer genes for CAZymes, targeting
492 primarily chitin and starch degradation. The Cloacimonadaceae were also predicted to be active
493 in acetogenic metabolisms, which likely support downstream methanogenesis (1, 30).

494 The abundance of genes associated with fermentative processes was significantly higher
495 overall in Newer cells. This included CAZymes for the breakdown of many polysaccharides and

genes associated with SCFA and alcohol conversion (Figure 2). Further supporting the predominance of fermentative metabolism, Newer cells had a near absence of genes associated with complexes I - IV of the electron transport chain, which are necessary for respiration (Figure 5).

During phase 3 (represented by Newer cells), rapid methanogenesis is the dominant process, utilizing breakdown products from the anaerobic acid phase (*e.g.*, SCFAs). Methane was being generated in all Newer cells, with large decreases in total gas flared in Intermediate and Older cells relative to Newer cells (explored in greater detail in Grégoire *et al.* [1]). In keeping with this, Grégoire *et al.* (1) found a higher proportion of putative methanogens in Newer and Intermediate cells than in Older cells. Supporting this shift in microbial metabolism, we also observed large decreases in BOD, COD, TOC, and SCFAs, consistent with microbial consumption of labile carbon sources and a likely transition from fermentation-based processes to predominantly methanogenesis early in the landfill life cycle, corresponding to the shift from phase 2 to 3 (Figure 5).

During phase 4, total gas production tends to decrease, but methanogenesis proceeds (4, 7, 33). Reduced concentrations of SCFAs and other more labile carbon substrates by this phase lead microbes to rely on degradation of more complex OM, a slower process that reduces overall methane production. In our data, Intermediate-aged cells (D1 and D2) had more recently entered phase 4, while Older cell C was also classified to this phase. In all phase 4 cells (C and D), total gas production was substantially lower than in phases 2-3 (Newer cells) but still dominated by methanogenesis. We also observed a decrease in the abundance of genes or functional gene groups associated with fermentative functions and a corresponding increase in MAGs carrying genes that confer metabolic flexibility across a variety of redox processes.

519 Cell C exhibited higher abundance of functional genes and gene groups associated with
520 redox cycling of Fe, N and S than D1/ D2, reflecting the shift toward metabolic flexibility by the
521 end of the phase 4, as methanogenesis continues to slow (Figure 3; Figure 5). Interestingly, we
522 also observed overall lower leachate concentrations of N, S, and Fe by phase 4, indicating a shift
523 in microbial metabolism to lithoautotrophy as methanogenesis slowed and conditions became
524 less reducing (Figure 5b). These changes in functional potential were in large part due to shifts in
525 microbial community composition between cells D1/D2 and cell C. Cell C, representing a later
526 portion of phase 4, was broadly dominated by 2 MAGs from the genus *Aliarcobacter* (44.0%
527 relative abundance). In particular, the genomes of these MAGs encoded genes related to
528 denitrification (nitrate > nitrite > nitric oxide), N fixation, degradation of carbon sources
529 (polyphenolics, chitin, mixed-linkage glucans), oxidation of thiosulfate, and several genes related
530 to acetate metabolism (acetate kinase, phosphate acetyltransferase, acetate--CoA ligase [ADP-
531 forming] subunit alpha). The potential for metabolic flexibility, something documented across
532 the Arcobacteraceae family (34, 35) may explain the predominance of this group in cell C. This
533 metabolic flexibility may give them a competitive advantage as biological activity declines
534 throughout phase 4.

535 Phase 5 of the landfill life cycle, called the stabilization or maturation phase by some and
536 the humic phase by others, is characterized by an increased potential for oxygen buildup and
537 oxidative processes, as well as organic matter that is largely recalcitrant (*e.g.*, humic and fulvic
538 acids) (6–8). Because this phase may take decades to develop, few studies have investigated
539 microbial communities and leachate geochemical conditions in detail. By phase 5, we observed
540 an overall decline in carbon-associated parameters in leachate, including BOD, COD, TOC, and
541 concentrations of SCFAs. This decrease in BOD, COD, and the BOD to COD ratio is often seen

as indicative of the transition to "mature" landfill status (3, 5, 33). These declines also signify reduced overall biological activity, indicating reductions in rates of decomposition as landfill waste ages – a critical indicator of the stabilization phase. This reduction in decomposition may be linked to the observed increase in oxygen flared from Older cells at this site, indicating that a lower proportion of infiltrating oxygen is being consumed by microbes (1). This observed increase in oxygen, though still at low levels, has been proposed by several authors as an additional indicator of the stabilization phase (3, 4). We also observed an increase in oxidation-reduction potential across in this window, a further indicator of a shift toward more oxidizing conditions and processes in the later phases of the landfill life cycle.

Reflecting the decrease in biological oxygen demand, we observed fewer overall MAGs and lower diversity in Older cells (A, B, Cs) relative to Newer cells. Microbial communities in Older cells were relatively enriched in chemolithoautotrophs (*e.g.,* Gallionellaceae, Sulfurimonadaceae), contrasting with the variety of diverse putative heterotrophs observed in Newer cells. This shift from chemoorganoheterotrophs to chemolithoautotrophs was also observed by Sekhohola-Dlamini *et al.* (2020), who found that a 14-year old MSW landfill with higher total carbon and N was dominated by copiotrophs, while a nearby 36-year old landfill was dominated by lithotrophs (13). Taxonomic shifts were also reflected in differences in functional gene abundances between Older and Newer cells. As noted above, relative abundance of MAGs with genes associated with the fermentation of carbon sources was significantly lower in Older cells. Possibly associated with increases in oxygen availability, significantly more MAGs in Older cells had genes associated with electron transport chain complexes I-IV, indicating the potential for aerobic respiration under changing redox conditions. Furthermore, Older cells had more metabolically flexible microbial communities, with significantly higher relative abundance

565 of MAGs with genes for reduction and/or oxidation of Fe, N, and S. For example, members of
566 the genera *Gallionella* and *Sideroxyarcus* (formerly *Sideroxydans*), which were enriched in Older
567 cells, are widely known to oxidize ferrous iron (36–38). Similarly, members of two other
568 enriched genera, *Sulfuricurvum* and *Sulfurimonas*, contain members known to be metabolically
569 flexible, capable of utilizing a variety of reduced S compounds as electron donors and nitrate or
570 oxygen as electron acceptors (39–41). Concentrations of nitrate, nitrite, and sulfide in leachate
571 were all relatively low (generally < 5 mg/L across all time points), indicating either low levels
572 available in the landfilled waste, steady conversion/uptake rates by the microbial community, or
573 both. In contrast, concentrations of sulfate were relatively higher (> 10 mg/L) throughout the
574 landfill life cycle, with no significant differences between Newer and Older cells at the time of
575 sampling.

576 **3.2 Redox response across decades of landfill waste decomposition**

577 Ammonia-N, sulfate, and Fe concentrations in leachate spiked at different points in the
578 landfill life cycle. Each of these redox-associated metabolites was linked to different
579 biogeochemical cycles in our dataset. First, other studies have reported a spike in ammonia-N
580 midway through the landfill life cycle as organics are depleted, mobilizing N via hydrolysis of
581 proteins in OM (3, 5). We observed a similar trend, with ammonia-N broadly peaking with
582 conductivity, bicarbonate, potassium, and sodium at around 20 years of landfill waste age (Figure
583 5b - cluster 4). This peak in conductivity, bicarbonate, and base cations (K and Na) has been
584 observed elsewhere. Conductivity has been observed to increase in young and intermediate-aged
585 landfills as ions are released from breakdown of organic material (3, 6, 42). Contributing to
586 conductivity, bicarbonate tends to increase in leachate as degradation of organic material
587 produces CO_2, forming carbonic acid and ultimately, bicarbonate ions (42, 43).

A notable trend during the mobilization and then reduction in labile carbon substrates from 0 – 10 years was an increase in leachate concentrations of Fe, Ca, Cd, and Cr, with peaks occurring around 6-8 years. (Figure 5b – Cluster 2). Although mobilization of these elements may be linked to their pH and redox-dependent natures (3, 8), it is important to note that pH generally remained above 6 in all samples at all time points, a phenomenon observed in other landfills' anaerobic acid phase (14). It is therefore unlikely that mobilization of Fe, Ca, Cd, and Cr is entirely pH-dependent, as the measured pH was not acidic enough to release these metals into solution. Instead, it is possible that metals formed soluble complexes or colloids with OM, increasing leachate concentrations relative to the later parts of the landfill life cycle (3). Furthermore, reducing conditions in the anaerobic phases may have influenced metal mobility, reducing, for example, Fe(III) to soluble Fe(II) (14). Further study is needed to fully understand the links between organic chemistry and metal cycling in landfill leachate over time.

Finally, concentrations of sulfate, Cu, Mg, Ni, and Zn, were all linked to the historic practice of leachate recirculation at the site (Figure 4; Figure 5b). Leachate recirculation is common in MSW landfills, where it is used to raise moisture content and hasten anaerobic decomposition (3, 44). At our site, leachate recirculation was practiced until the end of 2009, with variable volumes recirculated in each cell monthly. Linear regression analysis revealed that the volume of leachate recirculated was negatively associated with redox and nitrite-N and positively with BOD, COD, sulfate, Cu Cr, Fe, Mg, Ni, and Zn over time. Outside of studies specifically investigating leachate recirculation in landfills (44, 45), few mention if the practice was performed at their sites or consider the broader impacts recirculation has on microbial guilds that control waste decomposition, making it difficult to put our results in context. From our data, we suggest that more reducing conditions (decreases in redox potential) are an expected response

611 to leachate recirculation, which is broadly associated with increased rates of fermentation of
612 organic matter, possibly leading to higher BOD and COD (44, 45). Increased moisture content,
613 brought about by recirculation of leachate, can also promote dissolution of metal-bearing
614 minerals (*e.g.*, Fe/Mn-oxides) and mobilize metals previously bound to solid phases – this is
615 particularly true for metals like Cu, Ni, and Zn that more readily solubilize or bind to organic
616 ligands, thus keeping them in the leachate solution (14). Increased moisture content in landfill
617 cells may also increase contact time, which can release a variety of ions from solid phases,
618 including metals and sulfate.

619 **3.2 Metal fate within a landfill**

620 Given concerns about the impact of increasingly oxidizing conditions on metal mobility
621 and metal leaching in landfills (4, 14), one of the goals of our study was to investigate changes in
622 metal availability and putative metal cycling over the landfill life cycle. As mentioned above, the
623 practice of leachate recirculation appeared to accelerate metal release into landfill leachate. Our
624 study identified a previously-unreported association between leachate recirculation and metal
625 concentrations, allowing an initial examination of this phenomenon. Leachate recirculation
626 ceased at this site in 2009, so we had more data for leachate recirculation from Older and
627 Intermediate cells (A, B, C, D1, D2), with cell E only filling from 1999 onwards, and cell F not
628 extant in 2009 (2014 start to filling). Overwhelmingly, metal concentrations were higher in A, B,
629 and C (all filled before 1993) at the time of filling than in D1 and D2 (filled between 1993 and
630 1998), possibly due to changes in waste streams and waste management practices over time.
631 More research is needed to investigate the impacts of leachate recirculation on metal mobility
632 and fate, as existing research focuses on recirculation's role in accelerating breakdown of OM.

We hypothesized that Older landfill cells would host microbial communities with a higher abundance of functional genes associated with utilization of inorganic electron acceptors and cycling of metals. We found that the abundance of metal resistance genes was significantly higher in Older cells relative to Newer. Many different genes for metal resistance (for As, Cd, Cu, Co, Cr, Fe, Ni, Se, Te) were significantly more abundant in Older cells than Newer cells, despite lower metal concentrations. Genes for Fe oxidation and reduction were the only metal metabolism genes with significantly higher proportional abundances in Older cells. Interestingly, outside of Fe-cycling, the majority of metal resistance and metal cycling genes or gene groups were encoded by lower abundance MAGs that were not part of the most dominant families in Older cells (Gallionellaceae and Sulfurimonadaceae). Genes for As resistance were some of the most ubiquitous in Older cells, present across a variety of taxa including many, but not all, Gallionellaceae and Sulfurimonadaceae MAGs, lineages which harbour As resistance genes in other environments (40, 46). Genes for As resistance have been found across a variety of environments (21), including deep groundwater systems (46) and permafrost (47). While metal exposure may partially explain the high incidence of metal resistance genes in Older cells, which had highest metal levels historically (48), some studies have seen little overlap between metal exposure and relevant metal-resistance genes (46, 49). It is possible that fluctuations in redox conditions within the solid material in Older landfill cells results in spatial differences in metal exposure that influence microbial community composition and functional gene profiles, but that is difficult to determine without sampling solid landfill waste. Our study provided a comprehensive look at a wide range of metals, and further study is needed to elucidate direct and indirect biogeochemical cycling pathways for landfill metals.

3.3 Conclusions

In our study, we examined microbial communities, functional genes, and leachate chemistry across a landfill's cells of varying ages (2-39 years). We also tracked changes in geochemical conditions across 36 years of landfill leachate chemistry data. We found that the early phases of the landfill life cycle were dominated by fermentative processes, with labile carbon declining over time. Conditions became more oxidizing over time, with evidence of oxygen buildup in Older cells. Microbial diversity declined with time, and there was a clear shift from fermentative processes to utilization of alternative electron donors and acceptors. Our results were largely consistent with studies that modelled potential biogeochemical cycles in landfills in the stabilization phase, having never recorded them (3, 4).

Leachate metal concentrations were influenced by OM content and historic leachate recirculation practices. Leachate recirculation was associated with increases in metal mobility and the potential for metal leaching out of the system, possibly linked to organo-metal complexes. Future research investigating organo-metal complexes and the ability of natural landfill decomposition to pull metals into solution would be an exciting new avenue to better understand metal fate in these environments, especially in conjunction with better modeling for how leachate recirculation-modified moisture regimes impact metal leaching and OM cycling.

Our conceptual model of the key processes and metabolisms over a landfill's life cycle provides a new framework, based on empirical data, and synthesizing physical processes with microbial impacts. We note that this landfill's cells were only at the beginning of the stabilization phase. The landfill should continue to be monitored for changes in geochemical conditions and microbial community succession over time to better understand the unexplored dynamics of this crucial, final stage in a landfill life cycle.

4.0 Materials and Methods

4.1 Site Description

The sampled site is a municipal landfill located in the northeastern United States (NEUS). The site is composed of six landfill cells (A, B, C, D, E, and F), two of which are divided into sub-cells (D into D1 and D2, and F into F1 and F2), each equipped with leachate collection systems. Previous work at this site classified the landfill cells using a five-phase conceptual model based on leachate chemistry and biogas data (1). Cell A, which received waste from 1980 to 1982, and Cell B, which received waste from 1982 to 1988, were both classified as in phase 5. Cell C, which received waste from 1988 – 1993 was classified into phase 4. The authors of this prior study identified evidence of oxygen intrusion into cells A and B, informing their classification into phase 5 of the landfill life cycle. The two subcells of cell D were filled at different times. D1 received waste from 1993 – 1998 and cell D2 from 1995 – 1998. Both were classified into phase 4, due primarily to low gas production relative to cells E and F. Cell E was filled from 1999 – 2014 and was classified into phase 3 (rapid methanogenesis) due to high gas output, mostly composed of methane. Cell F1 filled from 2014 up to the time of sampling (March 2019) and F2 from 2016 up to the time of sampling (March 2019). Both were identified as transitioning from phase 2 (anaerobic acid phase) to phase 3 due to variable gas production but still high proportions of methane (1). For this study, decreases in oxygen demand (BOD) and chemical oxygen demand (COD) at A, B, and to a lesser extent, C, relative to the other cells prompted us to classify A, B, and C as “Older”. Cells E, F1, and F2 were categorized as “Newer”, while D1 and D2 were labelled “Intermediate”.

4.2 Leachate sampling

In 2019, we collected leachate samples from each cell/sub-cell for shotgun metagenomic sequencing. One leachate monitoring well at each cell was purged of 2-3 well volumes, and one

litre of leachate was collected using a peristaltic pump. Leachate samples were stored on ice and transported to the lab before being filtered through a 0.22 µm Sterivex filter (Millipore Sigma, Burlington, MA) on the day of sampling. Filters were stored at -80°C until DNA extractions were performed. Detailed descriptions of DNA extraction, sequencing, filtering, assembly, binning, and taxonomic assignment can be found in Grégoire *et al.* 2023 (1), which exclusively explored the predicted methane-cycling populations across the landfill. The pipeline for microbial community analyses is described in brief below.

4.3 DNA sequencing and prior analyses

DNA was extracted from biomass on Sterivex filters using the PowerSoil DNA Isolation Kit (Qiagen) according to the manufacturer's protocols but with the filter added to the initial bead tube in place of soil, and with elution into 50 µL of final buffer. DNA was quality-checked using a NanoDrop 1000 (Thermo Scientific, Waltham, MA) and quantified using Qubit fluorimetry (Thermo Scientific, Waltham, MA). Extracted DNA was sent to The Centre for Applied Genomics in Toronto, Canada for shotgun metagenomic sequencing on an Illumina HiSeq machine with paired 2x150 bp reads. Acquired metagenomic reads were quality-trimmed with bbduk in the BBTools suite (https://sourceforge.net/projects/bbmap/) and Sickle v1.33 (50) prior to assembly using SPAdes3 v3.15.5 (51). Scaffolds were trimmed by length (≥ 2.5 kbp) and reads were mapped onto scaffolds using Bowtie2 v2.3.4.1 (52). Scaffolds were binned using three different binning algorithms (CONCOCT v0.4.0, MaxBin2 v2.2.6, MetaBAT2 v2.12.1) and bins were dereplicated using DAS Tool v 1.1.1 before quality-checking in CheckM v 1.0.13 (53–57). A total of 1,881 metagenome-assembled genomes (MAGs) were retained with >70% completion and <10% contamination. Relative abundance of MAGs was calculated using the mean coverage for unique scaffold identifiers within each genome bin. To evaluate the functional

726 potential of microbial communities, MAGs were annotated using Distilled and Refined
727 Annotation of Metabolism (DRAM) v1.0 (19) to look at a wide array of functional genes using
728 both sequence similarity and hidden Markov model (HMM) based detection.

729 **4.4 Data analyses**

730 All previous work by Grégoire *et al.* is outlined in brief in section 4.3 (1). For this study,
731 taxonomy was assigned to metagenome-assembled genomes (MAGs) using the Genome
732 Taxonomy Database Toolkit (GTDB-tk) r266 (15). Phylogenomic analysis for all MAGs was
733 performed using GToTree v1.6, using a suite of 25 hidden Markov models (HMMs) for bacteria
734 and archaea to identify single copy genes and generate a tree (58). 1,570 out of our 1,647 MAGs
735 were placed on the tree. The resultant tree was visualized using the Interactive Tree of Life tool
736 (59). To investigate similarity of MAGs across landfill cells, we utilized the dereplication tool
737 dRep, which uses Mash and genome-wide ANI (gANI) to create clusters of MAGs based on
738 pairwise comparisons, choosing a similarity cutoff of 99% (60).

739 The product file from DRAM was used to investigate the presence of genes associated
740 with central metabolism, carbon-cycling, nitrogen-cycling, and sulfur-cycling. DRAM combines
741 genes into functional gene groups based on the presence of key genes. For example, for the
742 function "acetate, pt 1" to be considered present, MAGs need to have genes for both phosphate
743 acetyltransferase and acetate kinase. We utilized these DRAM categories in all cases except the
744 SOX complex for oxidation of thiosulfate, which DRAM considers to be present if any *sox* gene
745 (*A, B, C, D, X, Y,* or *Z)* is present. Researchers have demonstrated that the presence of *soxXA,*
746 *soxB,* and *soxYZ* are necessary for partial oxidation of thiosulfate, with *soxCD* completing the
747 reaction (61). Accordingly, we decided to apply a stricter threshold than DRAM, considering the

combined presence of *soxA, soxB, soxX, soxY,* and *soxZ* as required to indicate the ability for partial or complete oxidation of thiosulfate.

DRAM also annotates metabolic pathways and multi-subunit complexes (*e.g.*, electron transport chain [ETC]) based on the proportion of genes present. We considered a pathway or complex to be present when over 70% of genes were present. We utilized HMM-based pipelines for Fe and As metabolism and resistance, using FeGenie (20) for iron and Dunivin *et al*.'s arsenic resistance and metabolism pipeline (21). FeGenie uses a library of curated HMMs to group iron-related functional genes, while Dunivin *et al.*'s pipeline looks for individual marker genes using their HMM set. We also utilized BacMet version 2.0 for targeted annotation of metal-resistance genes by looking for homologs to experimentally-confirmed genes from the BacMet database (22). Genes from the BacMet database were filtered to only those which were involved in metal resistance, excluding genes related to genes for antibiotic resistance. Because BacMet and the Dunivin *et al*. pipeline employ different methods, we retained hits from both, even if the genes overlapped (*e.g.*, *arsB* from Dunivin vs. *arsB* from BacMet). Further information on genes contributing to functional groups can be found in the documentation for the tools listed above (Table S2).

All subsequent data analyses, including statistics and generation of figures, were performed in R version 4.3.1 (2023-06-16 ucrt) (62). We separated data into three categories for downstream analysis: Older cells aged 31 – 39 years (cells A, B, and C) and Newer cells aged 3 – 20 years (cells E, F1, and F2). D1 and D2 (aged 24 – 26) were considered Intermediate and were not included in statistical analyses. Base R was used for statistical tests. The packages "phyloseq" and "microeco" were used for generating Venn diagrams of MAG overlap among categories and for producing relative abundance bar graphs (63, 64). Relative abundance was

calculated by summing the mean coverage for all MAGs at a given taxonomic level (*e.g.*, at the Family level). Similarly, functional gene abundance was calculated using the relative coverage of MAGs that possessed a given functional gene, group, or pathway. Due to the variety of tools used for annotating functional genes, we collapsed data into binary presence-absence data for each gene, pathway, or gene group. Therefore, if 3 MAGs in a cell had coverages of 1%, 2%, and 3%, and each possessed at least one *arsA* gene, the "abundance" of the functional gene would be 6%. Wilcoxon rank sum tests were used to determine differences in functional gene abundance and chemical parameters between Older and Newer cells. Finally, heatmaps of functional gene abundance were generated using the package "ggplot2" (65).

4.5 Leachate chemistry

Thirty-six years of leachate chemistry records were provided by the site owners, with all analyses performed by Brickhouse Environmental consultants. While many parameters were provided by the site owners, we selected the following as relevant to microbial function and showing variance over time; pH, oxidation-reduction potential, electrical conductivity, bicarbonate, BOD, COD, TOC, sulfate, sulfide, ammonia-N, nitrate-N, nitrite-N, organic acids (acetic acid, propionic acid, isobutyric acid, butyric acid, isovaleric acid, valeric acid), total phenolics, base cations (Ca, K, Mg, Na) and metals (As, Cd, Co, Cr, Cu, Fe, Mn, Ni, Se). As leachate chemistry has changed greatly over time for some cells, we reported chemistry both during the time of filling and in the 5 years prior to our sampling to capture shifts over time.

To investigate trends in geochemical parameters over time, we computed 5-year rolling averages across all cells by time since filling across all 36 years (year 0 – 36) of provided leachate data. Then, we computed z-scores for each parameter, transforming data to a mean of 0 and standard deviation of 1 so trends across parameters could be compared agnostic of units.

Using an elbow plot of within-cluster sum of squares to determine the optimum numbers of clusters (Figure S4), we clustered the z-score adjusted data into 8 k-means clusters (Table 2). Plots of 5-year rolling averages were developed using the "ggplot2" package in R (65). Finally, to investigate the impact of the historic practice of leachate recirculation on leachate geochemistry, we ran linear regressions on z-score scaled 5-year rolling averages for all cells across the time window for which there was active leachate recirculation (> 5 gallons of leachate/month).

Acknowledgements

We are sincerely grateful to the landfill site management (anonymity by request) and Brickhouse Environmental consulting for site access, aid with sampling, and provision of detailed monitoring records. We thank Dr. Jennifer Biddle and her lab group for hosting our team for sample processing prior to shipment. Thanks also to Dr. Nikhil George, Ms. Rebecca Co, and Dr. Alexandra Sauk for help with sampling, and to Dr. Nikhil George for his work with binning pipelines. This work was supported by an NSERC Discovery Grant (2016-03686) and an Ontario Early Research Award (ER19-15-228) to LAH. LAH was supported by a Tier II Canada Research Chair.

Data Availability

All data involved in this research are publicly available. Sequencing data have been deposited to NCBI under the BioProject PRJNA900590, with raw reads available on the SRA database. Geochemical data, microbial functional annotations, and microbial taxonomy data are all available in the Open Science Framework (https://doi.org/10.17605/OSF.IO/MSDB8). All R

code used for statistical analyses and to generate figures are also on the Open Science Framework.

CRediT authorship contribution statement

Kimber E. Munford: Data curation, formal analysis, investigation, methodology, visualization, writing – original draft, writing – review & editing. **Daniel S. Grégoire:** Data curation, formal analysis, investigation, methodology, software, writing – review & editing. **Laura A. Hug:** Conceptualization, data curation, funding acquisition, project administration, resources, software, supervision, writing – review & editing.

Conflict of interest statement

The authors declare that there are no conflicts of interest to disclose.

832 **References**

833 1. Grégoire DS, George NA, Hug LA. 2023. Microbial methane cycling in a landfill on a
834 decadal time scale. Nat Commun 14:7402.

835 2. Meyer-Dombard DR, Bogner JE, Malas J. 2020. A Review of Landfill Microbiology and
836 Ecology: A Call for Modernization With 'Next Generation' Technology. Front Microbiol
837 11:1127.

838 3. Kjeldsen P, Barlaz MA, Rooker AP, Baun A, Ledin A, Christensen TH. 2002. Present and
839 Long-Term Composition of MSW Landfill Leachate: A Review. Crit Rev Environ Sci
840 Technol 32:297–336.

841 4. Pohland FG, Harper SR. 1985. Critical review and summary of leachate and gas production
842 from landfills. United States Environmental Protection Agency (EPA).

843 5. Kulikowska D, Klimiuk E. 2008. The effect of landfill age on municipal leachate
844 composition. Bioresour Technol 99:5981–5985.

845 6. Wijekoon P, Koliyabandara PA, Cooray AT, Lam SS, Athapattu BCL, Vithanage M. 2022.
846 Progress and prospects in mitigation of landfill leachate pollution: Risk, pollution potential,
847 treatment and challenges. J Hazard Mater 421:126627.

848 7. Liu J, Gu Z, Wang X, Li Q. 2022. The molecular differences of young and mature landfill
849 leachates: Molecular composition, chemical property, and structural characteristic.
850 Chemosphere 287:132215.

851 8. Bozkurt S, Moreno L, Neretnieks I. 1999. Long-term fate of organics in waste deposits and
852 its effect on metal release. Sci Total Environ 228:135–152.

9. Östman M, Wahlberg O, Mårtensson A. 2008. Leachability and metal-binding capacity in ageing landfill material. Waste Manag 28:142–150.

10. Zainun MY, Simarani K. 2018. Metagenomics profiling for assessing microbial diversity in both active and closed landfills. Sci Total Environ 616–617:269–278.

11. Hosseini Beinabaj SM, Heydariyan H, Mohammad Aleii H, Hosseinzadeh A. 2023. Concentration of heavy metals in leachate, soil, and plants in Tehran's landfill: Investigation of the effect of landfill age on the intensity of pollution. Heliyon 9:e13017.

12. Kang K-H, Shin HS, Park H. 2002. Characterization of humic substances present in landfill leachates with different landfill ages and its implications. Water Res 36:4023–4032.

13. Sekhohola-Dlamini L, Selvarajan R, Ogola HJO, Tekere M. 2021. Community diversity metrics, interactions, and metabolic functions of bacteria associated with municipal solid waste landfills at different maturation stages. MicrobiologyOpen 10:e1118.

14. Kim H, Jang Y-C, Townsend T. 2011. The behavior and long-term fate of metals in simulated landfill bioreactors under aerobic and anaerobic conditions. J Hazard Mater 194:369–377.

15. Chaumeil P-A, Mussig AJ, Hugenholtz P, Parks DH. 2019. GTDB-Tk: a toolkit to classify genomes with the Genome Taxonomy Database. Bioinformatics 36:1925–1927.

16. Hug LA. 2026. Munford_NEUS_Landfill_metals. https://doi.org/10.17605/OSF.IO/MSDB8. Open Science Framework.

872 17. Seymour CO, Palmer M, Becraft ED, Stepanauskas R, Friel AD, Schulz F, Woyke T, Eloe-
873 Fadrosh E, Lai D, Jiao J-Y, Hua Z-S, Liu L, Lian Z-H, Li W-J, Chuvochina M, Finley BK,
874 Koch BJ, Schwartz E, Dijkstra P, Moser DP, Hungate BA, Hedlund BP. 2023. Hyperactive
875 nanobacteria with host-dependent traits pervade Omnitrophota. Nat Microbiol 8:727–744.

876 18. Srinivas P, Peterson SB, Gallagher LA, Wang Y, Mougous JD. Beyond genomics in
877 Patescibacteria: A trove of unexplored biology packed into ultrasmall bacteria. Proc Natl
878 Acad Sci U S A 121:e2419369121.

879 19. Shaffer M, Borton MA, McGivern BB, Zayed AA, La Rosa SL, Solden LM, Liu P, Narrowe
880 AB, Rodríguez-Ramos J, Bolduc B, Gazitúa MC, Daly RA, Smith GJ, Vik DR, Pope PB,
881 Sullivan MB, Roux S, Wrighton KC. 2020. DRAM for distilling microbial metabolism to
882 automate the curation of microbiome function. Nucleic Acids Res 48:8883–8900.

883 20. Garber AI, Nealson KH, Okamoto A, McAllister SM, Chan CS, Barco RA, Merino N.
884 2020. FeGenie: A Comprehensive Tool for the Identification of Iron Genes and Iron Gene
885 Neighborhoods in Genome and Metagenome Assemblies. Front Microbiol 11.

886 21. Dunivin TK, Yeh SY, Shade A. 2019. A global survey of arsenic-related genes in soil
887 microbiomes. BMC Biology 17:45.

888 22. Pal C, Bengtsson-Palme J, Rensing C, Kristiansson E, Larsson DGJ. 2014. BacMet:
889 antibacterial biocide and metal resistance genes database. Nucleic Acids Res 42:D737–
890 D743.

891 23. Kato S, Ogasawara A, Itoh T, Sakai HD, Shimizu M, Yuki M, Kaneko M, Takashina T,
892 Ohkuma M. 2022. *Nanobdella aerobiophila* gen. nov., sp. nov., a thermoacidophilic,

893 obligate ectosymbiotic archaeon, and proposal of *Nanobdellaceae* fam. nov., *Nanobdellales*
894 ord. nov. and *Nanobdellia* class. nov. Int J Syst Evol Microbiol 72:005489.

895 24. Kuroda K, Maeda R, Shinshima F, Urasaki K, Kubota K, Nobu MK, Noguchi TQP, Satoh
896 H, Yamauchi M, Narihiro T, Yamada M. 2024. Microbiological insights into anaerobic
897 phenol degradation mechanisms and bulking phenomenon in a mesophilic upflow anaerobic
898 sludge blanket reactor in long-term operation. Water Res 253:121271.

899 25. Co R, Hug LA. 2021. Prediction, enrichment and isolation identify a responsive,
900 competitive community of cellulolytic microorganisms from a municipal landfill. FEMS
901 Microbiol Ecol 97:fiab065.

902 26. Xu S, Lu W, Liu Y, Ming Z, Liu Y, Meng R, Wang H. 2017. Structure and diversity of
903 bacterial communities in two large sanitary landfills in China as revealed by high-
904 throughput sequencing (MiSeq). Waste Manag 63:41–48.

905 27. Hu L, Huang F, Qian Y, Ding T, Yang Y, Shen D, Long Y. 2024. Pathways and contributions
906 of sulfate reducing-bacteria to arsenic cycling in landfills. J Hazard Mat 473:134582.

907 28. Pecorini I, Rossi E, Becarelli S, Baldi F, Di Gregorio S, Iannelli R. 2023. Wet Anaerobic
908 Codigestion of Sewage Sludge and OFMSW in Pilot-Scale Continuously Stirred Tank
909 Reactors: Focus on the Reactor Microbial Communities. 4. Sustainability 15:3168.

910 29. Santinello D, Zampieri G, Agostini S, Müller B, Favaro L, Treu L, Campanaro S. 2024.
911 Process stability in anaerobic Digestion: Unveiling microbial signatures of full-scale reactor
912 performance. Chem Eng J 497:154962.

913 30. Johnson LA, Hug LA. 2022. Cloacimonadota metabolisms include adaptations in
914 engineered environments that are reflected in the evolutionary history of the phylum.
915 Environ Microbiol Rep 14:520–529.

916 31. Schwan B, Abendroth C, Latorre-Pérez A, Porcar M, Vilanova C, Dornack C. 2020.
917 Chemically Stressed Bacterial Communities in Anaerobic Digesters Exhibit Resilience and
918 Ecological Flexibility. Front Microbiol 11.

919 32. Dyksma S, Gallert C. 2019. Candidatus Syntrophosphaera thermopropionivorans: a novel
920 player in syntrophic propionate oxidation during anaerobic digestion. Environ Microbiol
921 Rep 11:558–570.

922 33. Luo H, Zeng Y, Cheng Y, He D, Pan X. 2020. Recent advances in municipal landfill
923 leachate: A review focusing on its characteristics, treatment, and toxicity assessment. Sci
924 Total Environ 703:135468.

925 34. Li J, Xiang S, Li Y, Cheng R, Lai Q, Wang L, Li G, Dong C, Shao Z. 2024.
926 Arcobacteraceae are ubiquitous mixotrophic bacteria playing important roles in carbon,
927 nitrogen, and sulfur cycling in global oceans. mSystems 9:e00513-24.

928 35. Buzzanca D, Kerkhof P-J, Alessandria V, Rantsiou K, Houf K. 2023. Arcobacteraceae
929 comparative genome analysis demonstrates genome heterogeneity and reduction in species
930 isolated from animals and associated with human illness. Heliyon 9:e17652.

931 36. Zhou N, Keffer JL, Polson SW, Chan CS. 2022. Unraveling Fe(II)-Oxidizing Mechanisms
932 in a Facultative Fe(II) Oxidizer, Sideroxydans lithotrophicus Strain ES-1, via Culturing,

933 Transcriptomics, and Reverse Transcription-Quantitative PCR. Appl Environ Microbiol
934 88:e01595-21.

935 37. Kato S, Itoh T, Iino T, Ohkuma M. 2022. Sideroxyarcus emersonii gen. nov. sp. nov., a
936 neutrophilic, microaerobic iron- and thiosulfate-oxidizing bacterium isolated from iron-rich
937 wetland sediment. Int J Syst Evol Microbiol 72:005347.

938 38. Hallbeck L, Pedersen K. 2014. The Family Gallionellaceae, p. 853–858. *In* Rosenberg, E,
939 DeLong, EF, Lory, S, Stackebrandt, E, Thompson, F (eds.), The Prokaryotes. Springer
940 Berlin Heidelberg, Berlin, Heidelberg.

941 39. Han Y, Perner M. 2015. The globally widespread genus Sulfurimonas: versatile energy
942 metabolisms and adaptations to redox clines. Front Microbiol 6.

943 40. Handley KM, Bartels D, O'Loughlin EJ, Williams KH, Trimble WL, Skinner K, Gilbert JA,
944 Desai N, Glass EM, Paczian T, Wilke A, Antonopoulos D, Kemner KM, Meyer F. 2014.
945 The complete genome sequence for putative H2- and S-oxidizer Candidatus Sulfuricurvum
946 sp., assembled de novo from an aquifer-derived metagenome. Environ Microbiol 16:3443–
947 3462.

948 41. Kodama Y, Watanabe K. 2004. Sulfuricurvum kujiense gen. nov., sp. nov., a facultatively
949 anaerobic, chemolithoautotrophic, sulfur-oxidizing bacterium isolated from an underground
950 crude-oil storage cavity. Int J Syst Evol Microbiol 54:2297–2300.

951 42. Naveen BP, Mahapatra DM, Sitharam TG, Sivapullaiah PV, Ramachandra TV. 2017.
952 Physico-chemical and biological characterization of urban municipal landfill leachate.
953 Environ Pollut 220:1–12.

43. Christensen TH, Kjeldsen P, Bjerg PL, Jensen DL, Christensen JB, Baun A, Albrechtsen H-J, Heron G. 2001. Biogeochemistry of landfill leachate plumes. Appl Geochem 16:659–718.

44. Chan GYS, Chu LM, Wong MH. 2002. Effects of leachate recirculation on biogas production from landfill co-disposal of municipal solid waste, sewage sludge and marine sediment. Environ Pollut 118:393–399.

45. Zheng J, Wang X-G, Sun Y, Wang Y-X, Sha H-Q, He X-S, Sun X-J. 2024. Natural and anthropogenic dissolved organic matter in landfill leachate: Composition, transformation, and their coexistence characteristics. J Hazard Mat 465:133081.

46. Chen M, Grégoire DS, St-Germain P, Berdugo-Clavijo C, Hug LA. 2025. Microbial diversity and capacity for arsenic biogeochemical cycling in aquifers associated with thermal mobilization. Sci Total Environ 977:179357.

47. Mindlin S, Petrenko A, Kurakov A, Beletsky A, Mardanov A, Petrova M. 2016. Resistance of Permafrost and Modern Acinetobacter lwoffii Strains to Heavy Metals and Arsenic Revealed by Genome Analysis. Biomed Res Int 2016:3970831.

48. Roosa S, Wattiez R, Prygiel E, Lesven L, Billon G, Gillan DC. 2014. Bacterial metal resistance genes and metal bioavailability in contaminated sediments. Environ Pollut 189:143–151.

49. Ayala-Muñoz D, Burgos WD, Sánchez-España J, Couradeau E, Falagán C, Macalady JL. 2020. Metagenomic and Metatranscriptomic Study of Microbial Metal Resistance in an Acidic Pit Lake. Microorganisms 8:1350.

50. Joshi N, Fass J. 2025. Sickle: a sliding-window, adaptive, quality-based trimming tool for FastQ files (Version 1.33).

51. Prjibelski A, Antipov D, Meleshko D, Lapidus A, Korobeynikov A. 2020. Using SPAdes De Novo Assembler. Curr Protoc Bioinformatics 70:e102.

52. Langmead B, Salzberg SL. 2012. Fast gapped-read alignment with Bowtie 2. Nat Methods 9:357–359.

53. Parks DH, Imelfort M, Skennerton CT, Hugenholtz P, Tyson GW. 2015. CheckM: assessing the quality of microbial genomes recovered from isolates, single cells, and metagenomes. Genome Res 25:1043–1055.

54. Sieber CMK, Probst AJ, Sharrar A, Thomas BC, Hess M, Tringe SG, Banfield JF. 2018. Recovery of genomes from metagenomes via a dereplication, aggregation and scoring strategy. Nat Microbiol 3:836–843.

55. Alneberg J, Bjarnason BS, de Bruijn I, Schirmer M, Quick J, Ijaz UZ, Lahti L, Loman NJ, Andersson AF, Quince C. 2014. Binning metagenomic contigs by coverage and composition. Nat Methods 11:1144–1146.

56. Wu Y-W, Simmons BA, Singer SW. 2016. MaxBin 2.0: an automated binning algorithm to recover genomes from multiple metagenomic datasets. Bioinformatics 32:605–607.

57. Kang DD, Froula J, Egan R, Wang Z. 2015. MetaBAT, an efficient tool for accurately reconstructing single genomes from complex microbial communities. PeerJ 3:e1165.

58. Lee MD. 2019. GToTree: a user-friendly workflow for phylogenomics. Bioinformatics 35:4162–4164.

59. Letunic I, Bork P. 2021. Interactive Tree Of Life (iTOL) v5: an online tool for phylogenetic tree display and annotation. Nucleic Acids Res 49:W293–W296.

60. Olm MR, Brown CT, Brooks B, Banfield JF. 2017. dRep: a tool for fast and accurate genomic comparisons that enables improved genome recovery from metagenomes through de-replication. ISME J 11:2864–2868.

61. Friedrich CG, Rother D, Bardischewsky F, Quentmeier A, Fischer J. 2001. Oxidation of Reduced Inorganic Sulfur Compounds by Bacteria: Emergence of a Common Mechanism? Appl Environ Microbiol 67:2873–2882.

62. R Core Team. 2023. R: A language and environment for statistical computing. manual. R Foundation for Statistical Computing, Vienna, Austria.

63. McMurdie PJ, Holmes S. 2013. phyloseq: An R Package for Reproducible Interactive Analysis and Graphics of Microbiome Census Data. PLoS One 8:e61217.

64. Liu C, Cui Y, Li X, Yao M. 2021. microeco: An R package for data mining in microbial community ecology. FEMS Microbiol Ecol 97:fiaa255.

65. Wickham H. 2016. ggplot2: Elegant graphics for data analysis. Springer-Verlag New York.

Figures

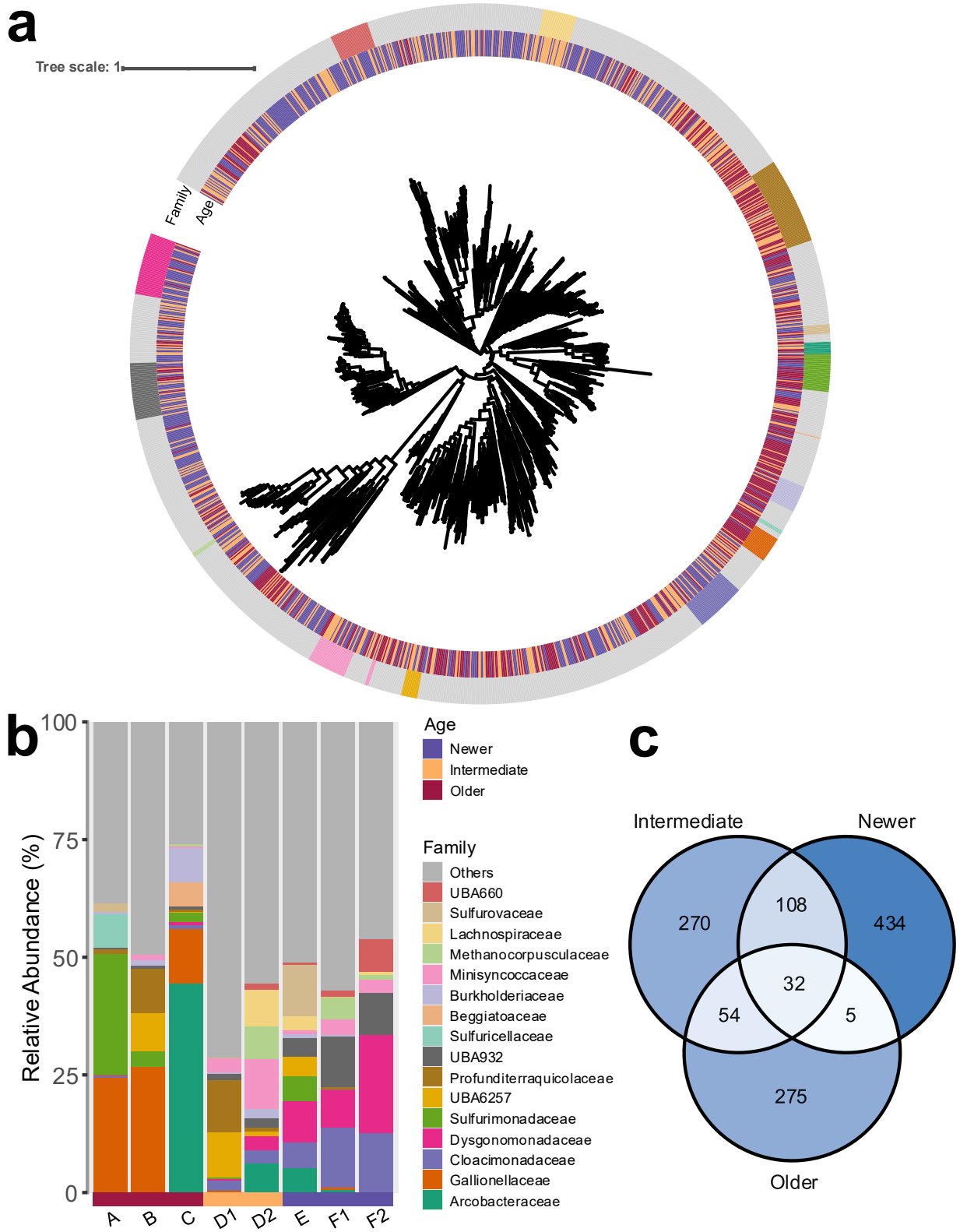
a
Tree scale: 1
Family
Age
b
Relative Abundance (%)
100
75
50
25
0
A
B
C
D1
D2
E
F1
F2
Age
Newer
Intermediate
Older
Family
Others
UBA660
Sulfurovaceae
Lachnospiraceae
Methanocorpusculaceae
Minisyncoccaceae
Burkholderiaceae
Beggiatoaceae
Sulfuricellaceae
UBA932
Profunditerraquicolaceae
UBA6257
Sulfurimonadaceae
Dysgonomonadaceae
Cloacimonadaceae
Gallionellaceae
Arcobacteraceae
c
Intermediate
Newer
Older
270
108
434
32
54
5
275

1015 **Figure 1: a) Phylogenomic tree based on 25 target gene HMMs for bacteria and archaea,**
1016 **placing 1,570 out of 1,647 MAGs in relation to each other, generated in GToTree v1.6** (58)**.**
1017 Rings depict, outer to inner: 1) family-level taxonomy, 2) cell age category. MAGs in the tree
1018 were not dereplicated so that sample-specific relative abundances could be depicted. Colours for
1019 families correspond to those in the b) barplot of relative abundance of all bacterial and archaeal
1020 families with over 5% relative abundance in at least one landfill cell, with lower abundance
1021 lineages grouped under "Other". Taxonomy was taken from GTDB-tk r266, where lineages
1022 starting with UBA are officially recognized but not yet formally named. c) Venn diagram
1023 indicating counts and percentages of shared MAGs (clustered at 99% similarity using DRep)
1024 among age categories across landfill cells. Venn sections are colored by proportion of MAGs
1025 within a category, with higher values corresponding to darker colors.

1026

1027

1028 **Figure 2: Carbon cycling differential abundance across landfill cells.** Heatmap depicting the
1029 summed relative coverage of all MAGs in each landfill cell that contain genes associated with

specific functions within carbon cycling. Only genes/pathways/processes which had significantly different abundances between Older and Newer cells (Wilcoxon rank sum test, Benjamini-Hochberg-corrected p-value of $p < 0.05$) are displayed. Boxes indicate whether abundance was significantly higher in Newer or Older cells. Central C metabolism pathways from DRAM were required to be >70% complete within a MAG for inclusion. Carbohydrate-active enzymes from DRAM either indicate the presence of genes for both backbone and oligomer cleavage (alpha-mannan, arabinan, beta-galactan, mixed-linkage glucans, pectin, starch, sulf-polysaccharides, xyloglucan) or only oligomer cleavage (arabinose cleavage, fucose cleavage, rhamnose cleavage). For polyphenolics, multiple oxidative genes are accounted for. For DRAM SCFA and alcohol conversions, the gene(s) of interest are listed in brackets. Further information can be found in the DRAM documentation.

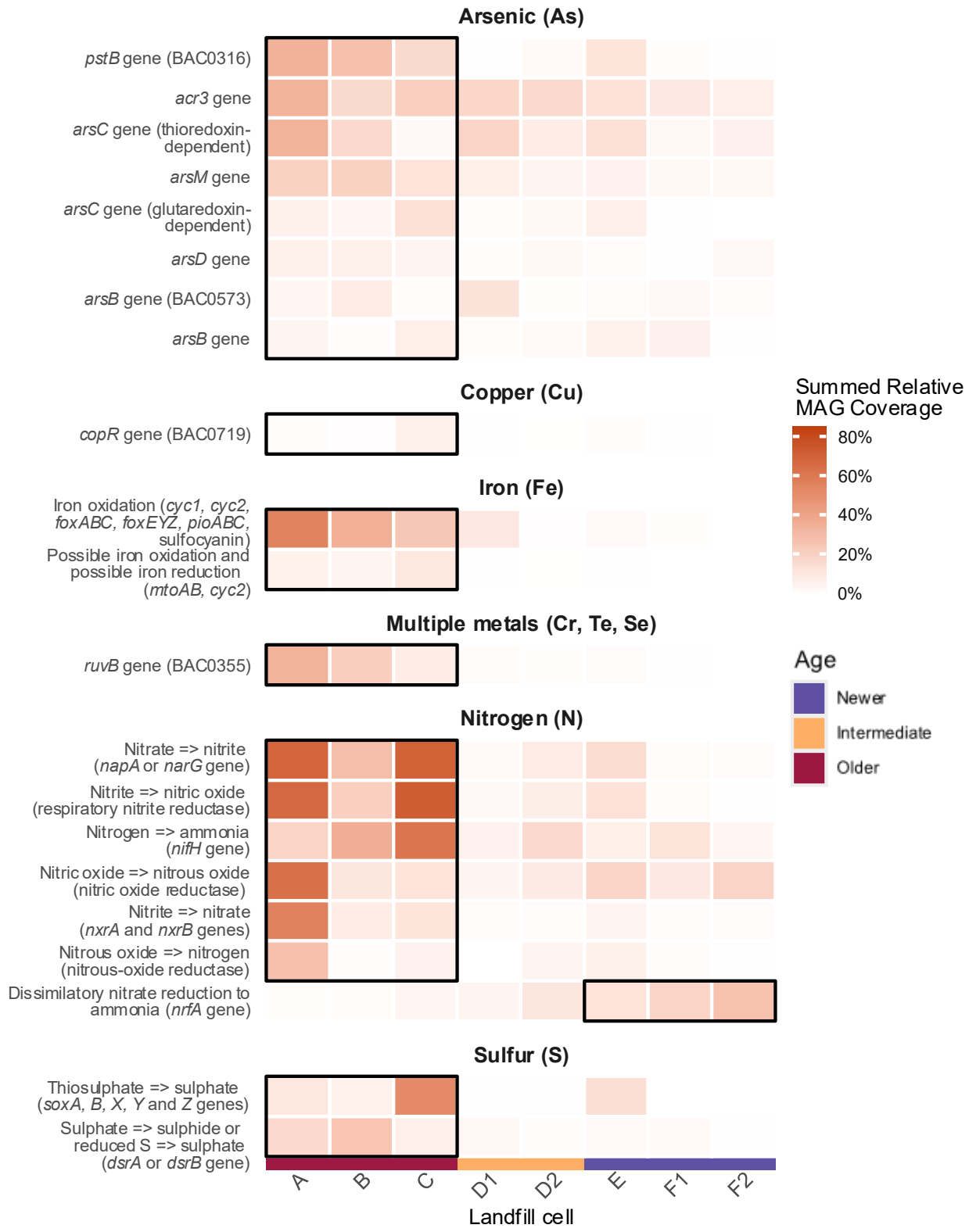

1043

1044 **Figure 3: Redox cycling and metal resistance differential abundance across landfill cells.**
1045 Heatmap depicting the summed relative coverage of all MAGs in each cell that contain

genes/processes associated with specific functions within redox cycling and metal resistance. Only genes/processes which had significantly different abundances between Older and Newer cells (Wilcoxon rank sum test, Benjamini-Hochberg-corrected p-value of $p < 0.05$) are displayed. Genes/processes with a maximum of < 0.05% relative coverage were pruned for clarity and are presented in Figure S3. Genes and functional groups come from four tools: FeGenie and an HMM set from Dunivin et al. for Fe and As, respectively, BacMetScan for metal-resistance genes and DRAM for functional groups associated with S and N cycling. For As-related genes detected using the Dunivin et al. HMM set, the gene of interest is listed. For BacMetScan annotations, the BacMet number is listed in brackets following the gene. For FeGenie annotations, the process is listed, followed by the relevant genes in brackets. Finally, for DRAM annotations, the process is listed, followed by the gene(s) of interest in brackets.

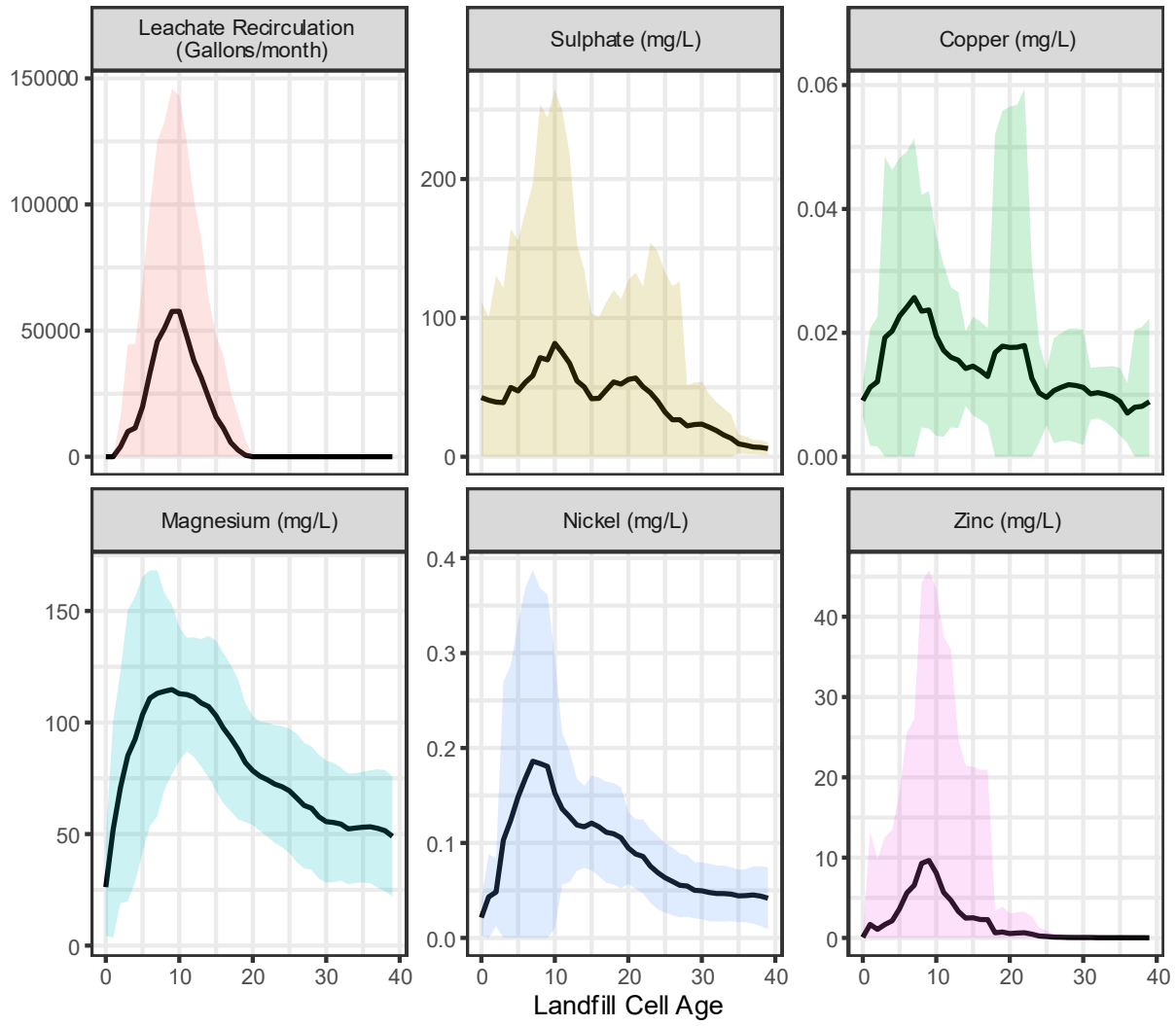

Figure 4: Line graphs depicting the 5-year rolling average (line) and standard deviation (shaded band around line) for landfill leachate parameters across 36 years of leachate chemistry data. All depicted parameters were within one k-means cluster (cluster 1).

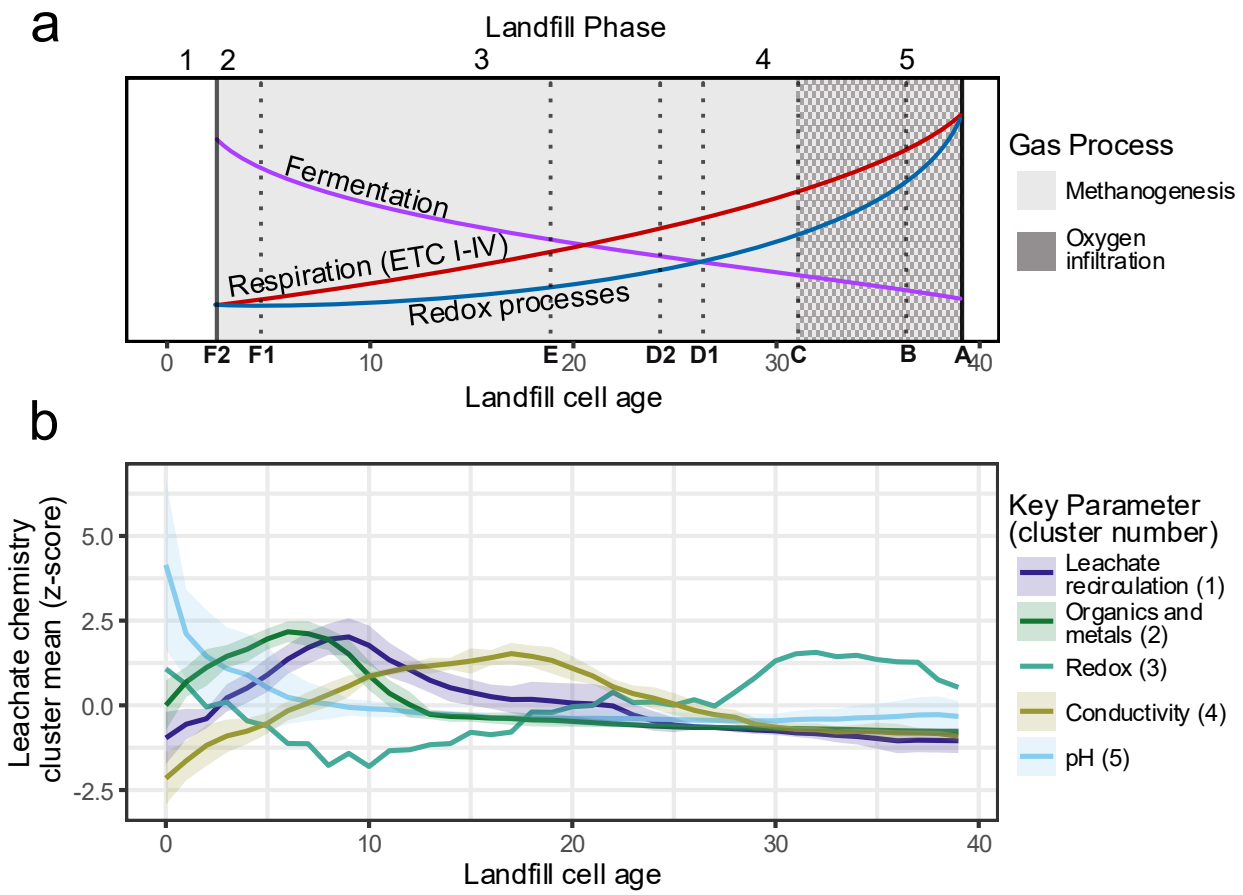

Figure 5: Conceptual diagram of landfill processes over time and landfill phases. a) Trends in functional gene groups over landfill cells varying in age from 3 to 39 years across 4 landfill phases, overlaid on predicted methane/O_2 dynamics. Solid lines represent the beginning and end of our observations, and the dashed lines represent the ages at which all other cells were sampled. Landfill phases are depicted along the top, but it is notable that cells F1 and F2 (the two newest cells) were transitioning from phase 2 to 3. Trend lines represent three functional gene groups: Fermentation (SCFA/alcohol degradation, carbohydrate-active enzymes), Respiration (defined by abundance of complete (>70% of constituent genes present) electron transport chain complexes for ETC I-IV) and Redox Processes (comprising genes for redox transformations of Fe, N, S, and As). Gas dynamics are depicted as greyscale background, with methane dominating an anoxic environment from years 3-26, followed by oxygen infiltration in later years. b) Line graph depicting trends in key geochemical variables across 36 years of leachate chemistry data. Lines depict the means of all z-score-adjusted parameters within a given k-means cluster, with standard deviation of all z-score adjusted parameters within a cluster indicated by lighter bands. Clusters are named in the legend based on their key physical variable(s). Note that redox has no standard deviation because it was the sole member of its cluster (Cluster 3).

Tables

Table 1: All geochemical measurements (mean±sd) for key variables, collated by landfill cell age class during filling of the cells and during the 5 years prior to sampling in winter 2019. Benjamini-Hochberg corrected p-values are presented for Wilcoxon rank sum comparisons between age classes in the 5 years prior to sampling. Only parameters that were significantly different at $p < 0.05$ are presented here. Remaining variables can be seen in Table S3.

Analyte	Older (A, B, C)	Newer (E, F1, F2)	Benjamini - Hochberg corrected p - value
Conductivity (µs/cm)	4665 ± 2083	7789 ± 3629	< 0.001
Redox (mV)	-36.1 ± 71.8	-88.8 ± 69.5	< 0.001
Bicarbonate (mg/L)	1557 ± 774	1842 ± 1242	0.00257
BOD_5 (mg/L)	71.6 ± 194.2	251 ± 308	< 0.001
COD (mg/L)	446 ± 387	1052 ± 875	< 0.001
TOC (mg/L)	115 ± 56.2	272 ± 227	< 0.001
Sulfide (mg/L)	0.845 ± 0.471	5.17 ± 11.4	< 0.001
Ammonia-N (mg/L)	219 ± 123	458 ± 306	< 0.001
Acetic acid (mg/L)	12.2 ± 25.1	61.3 ± 71.4	< 0.001
Propionic acid (mg/L)	9.99 ± 21.5	34.2 ± 72.4	0.0151
Total phenolics (mg/L)	0.173 ± 0.183	0.835 ± 1.59	< 0.001
Arsenic (µg/L)	16.9 ± 14.5	61.4 ± 61.4	< 0.001
Chromium (µg/L)	6.17 ± 4.12	56.8 ± 53.8	< 0.001
Iron (mg/L)	29.4 ± 101	51.8 ± 52.1	< 0.001
Manganese (mg/L)	0.418 ± 0.494	1.29 ± 1.51	< 0.001
Nickel (µg/L)	38.5 ± 26.5	110 ± 79.8	< 0.001
Calcium (mg/L)	67.6 ± 17.3	141 ± 89.3	< 0.001
Magnesium (mg/L)	48.0 ± 23.4	91.8 ± 42.8	< 0.001
Potassium (mg/L)	195 ± 94.4	242 ± 137	0.00194
Sodium (mg/L)	469 ± 226	736 ± 422	< 0.001

Table 2: Cluster membership for 8 k-means clusters of z-score adjusted 5-year rolling averages of 36 years of landfill leachate data.

Cluster number	Key parameter	All parameters
1	Leachate recirculation	Leachate recirculation, sulfate, Cu, Mg, Ni, Zn
2	Organics and metals	BOD-5, COD, TOC, organic acids (acetic acid, propionic acid, isobutyric acid, butyric acid, isovaleric acid, valeric acid), total phenolics, Ca, Cd, Cr, Fe
3	Redox	Redox (oxidation-reduction potential)
4	Conductivity	Conductivity, sulfide, ammonia-N, bicarbonate, As, K, Na
5	pH	pH, Mn
6	Nitrite-N	Nitrite-N
7	Nitrate-N	Nitrate-N, Se
8	Cobalt	Co